



Preparation and characterization of porous NiTi alloys synthesized by microwave sintering using Mg space holder

Tao LAI¹, Ji-lin XU¹, Qi-fei XIAO¹, Yun-xiang TONG²,
Jun HUANG¹, Jian-ping ZHANG¹, Jun-ming LUO¹, Yong LIU³

1. School of Materials Science and Engineering, Nanchang Hangkong University, Nanchang 330063, China;
2. Center for Biomedical Materials and Engineering, Harbin Engineering University, Harbin 150001, China;
3. Key Laboratory of Lightweight and High Strength Structural Materials of Jiangxi Province, Nanchang University, Nanchang 330031, China

Received 27 February 2020; accepted 9 November 2020

Abstract: To obtain the lightweight, high strength, and high damping capacity porous NiTi alloys, the microwave sintering coupled with the Mg space holder technique was employed to prepare the porous NiTi alloys. The microstructure, mechanical properties, phase transformation behavior, superelasticity, and damping capacity of the porous NiTi alloys were investigated. The results show that the porous NiTi alloys are mainly composed of the *B2* NiTi phase with a few *B19'* NiTi phase as the sintering temperature is lower than or equal to 900 °C. With increasing the sintering temperature, the porosities of the porous NiTi alloys gradually decrease and the compressive strength increases first, reaching the maximum value at 900 °C, and then decreases. With increasing the Mg content from 1 wt.% to 7 wt.%, the porosities of the porous NiTi alloys increase from 37.8% to 47.1%, while the compressive strength decreases from 2058 to 1146 MPa. Compared with the NH_4HCO_3 space holder, the phase transformation behavior of the porous NiTi alloys prepared with Mg space holder changes, and all of the compressive strength, superelasticity, shape memory effect and damping capacity are greatly improved.

Key words: porous NiTi alloy; microwave sintering; Mg space holder; superelasticity; damping capacity

1 Introduction

Nickel–titanium shape memory alloys (NiTi SMAs) have been widely used in aerospace, petrochemical, marine engineering, biological application, construction and other fields due to their unique shape memory effect and super-elasticity as well as high corrosion resistance, excellent biocompatibility and superior damping capacity [1–3]. Recently, porous NiTi alloys have been attracting more attention because the introduction of pore structure into the alloys can reduce the density and elastic modulus of the alloys,

which is very beneficial for mass reduction in aerospace [4] and for avoiding the stress shielding effect in orthopedics [5]. The powder metallurgy coupled with the space holder technique has been considered as one of the most effective methods to fabricate the porous metallic materials with tailored porosities and pore geometries [6].

Many powder metallurgy methods have been employed to fabricate the porous NiTi alloys by far, including conventional sintering (CS) under the vacuum or the atmosphere protection [7,8], self-propagating high-temperature synthesis (SHS) [9], hot isostatic pressing (HIP) [10], spark plasma sintering (SPS) [11] and microwave sintering

Corresponding author: Ji-lin XU, Tel: +86-791-83863034, E-mail: jlxu@nchu.edu.cn;

Jun-ming LUO, Tel: +86-791-83953271, E-mail: ljmniat@126.com

DOI: 10.1016/S1003-6326(21)65511-5

1003-6326/© 2021 The Nonferrous Metals Society of China. Published by Elsevier Ltd & Science Press

(MWS) [2,12,13]. Unfortunately, the undesired secondary phases (Ni_3Ti and Ti_2Ni) were detected in almost all of the sintering methods using the elemental powders to prepare the porous NiTi alloys due to the insufficient diffusion during sintering [14,15]. On the other hand, a large number of space holder materials have been also employed, such as ammonium hydrogen carbonate (NH_4HCO_3) [7,11,12], urea ($\text{CO}(\text{NH}_2)_2$) [16], sodium chloride (NaCl) [17] or sodium fluoride (NaF) [18], magnesium powder (Mg) [14,19,20] and other organic particles [21,22]. However, the soluble inorganic salts (NaCl or NH_4HCO_3) as the space holder materials always need additional steps of processing, such as dissolution for NaCl and precalculation for NH_4HCO_3 . In addition, premature decomposition or volatilization of space holder particles leads to the formation of a large number of macropores, which greatly increases the diffusion path of Ni and Ti atoms and leads to the increase of the secondary phases [23]. Among the space holder materials, the Mg powders have many advantages. Firstly, no separate removal step is required for Mg powders to form pores through their evaporation during the sintering process. Secondly, Mg vapor can provide a reducing atmosphere to prevent oxidation of titanium [14]. Thirdly, even the partial residue of Mg does not affect the properties of titanium alloy, and is even beneficial to its biocompatibility [24].

Recently, the porous NiTi alloy has been prepared using the Mg space holder with the pre-alloyed NiTi powders to prevent the formation of the undesired secondary phases [14,19,20]. Except for the above-mentioned effects, other functions of Mg for in-situ synthesis of porous NiTi alloy using elemental powders have been neglected. In this work, the porous NiTi alloys were prepared by microwave sintering using elemental Ni and Ti powders as the raw materials coupled with the Mg powders as the space holder particles. At the same time, the effects of sintering temperatures and Mg contents on the porosities, pore size distributions, densities, phase compositions and compression properties of porous NiTi alloy were investigated. The phase transformation behavior, superelasticity and shape memory effect and damping capacity of the porous NiTi alloys were also evaluated. Moreover, in structural characterization and performance tests, two other porous NiTi samples

prepared without using the space holder and using NH_4HCO_3 space holder were as the control samples.

2 Experimental

2.1 Raw materials

Commercially available pure dehydrated titanium (Ti) powders and carbonyl nickel (Ni) powders with the nominal mole ratios of 49.2% to 50.8% were used as the raw materials, in which the Ti powders had the particle size $\leq 45 \mu\text{m}$ and the purity $\geq 99.5\%$, and the Ni powders had the particle size $\leq 2 \mu\text{m}$ and the purity $\geq 99.7\%$. Mg powders and ammonium hydrogen carbonate (NH_4HCO_3) powders were chosen as the space holder materials, and both the Mg powders and NH_4HCO_3 powders had the particle size $\leq 150 \mu\text{m}$. All of the Ti, Ni and Mg powders were purchased from Beijing Xingrongyuan Technology Co., Ltd, China, and the NH_4HCO_3 powders were purchased from Tianjin Hengxing Chemical Reagent Co., Ltd., China.

2.2 Preparation of porous NiTi alloys

The Ti–50.8at.%Ni mixed powders with the different Mg powder contents (1, 3, 5 and 7 wt.%, the sintered samples noted as NiTi–xMg) were blended in a planetary ball mill (QM–3SP4, Nanjing University Instrument Plant, China) at a speed of 250 r/min for 3 h. To prevent the oxidation of powders and maintain the sizes and shapes of the space holder agent, no balls were added in the process of ball milling. The blended Ni–Ti–Mg powders were cold-pressed into green compacts ($d11.5 \text{ mm} \times 8 \text{ mm}$ and $50 \text{ mm} \times 6 \text{ mm} \times 6 \text{ mm}$) under a uniaxial pressure of 775 MPa for 1 min. Then, the green compacts were put into a 2.45 GHz, 5 kW microwave sintering furnace (NJZ4-3, Nanjing Jiequan Co., Ltd., China), and the schematic diagram of the process for preparing porous NiTi alloys and the microwave sintering setup is shown in Fig. 1. The green compact samples were sintered by microwave heating at a rate of $15 \text{ }^\circ\text{C}/\text{min}$ to 800, 850, 900 and $950 \text{ }^\circ\text{C}$ for 15 min, respectively, and cooled in furnace down to room temperature. For comparison, the Ni–Ti compact without adding space holder material (the sintered sample noted as NiTi–0Mg) and Ni–Ti–10wt.% NH_4HCO_3 compact (the sintered sample noted as NiTi–10N) were prepared and sintered

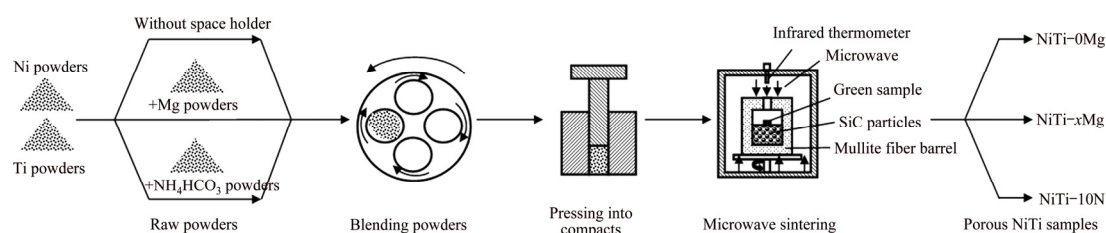


Fig. 1 Schematic diagram of process for preparing porous NiTi alloys

under the same process at 900 °C for 15 min. During the sintering process, the microwave sintering furnace was filled with flowing high purity argon gas (purity >99.999%) to prevent the oxidation of the sintered samples.

2.3 Microstructural characterization

The pore structure of the porous NiTi alloys was characterized by optical microscopy (DM1500, Shenzhen Hipower Optoelectronics Co., Ltd., China). The phase composition of the porous NiTi alloys was identified by X-ray diffraction (XRD, Bruker D8 FOCUS, Germany). The actual porosity (P) of the porous NiTi alloys was investigated by the Archimedes' principle according to ASTM B962–08, in which the theoretical density of the NiTi alloys was 6.45 g/cm³. The pore size distributions of the porous NiTi alloys were analyzed by the software of Image-Pro Plus version 6.0.

2.4 DSC test

The phase transformation behavior of the porous NiTi alloys was analyzed using a Perkin–Elmer Diamond differential scanning calorimeter (DSC) with a heating/cooling rate of 20 °C/min. The mass of the test samples was 10–20 mg, and the test temperature range was from –80 to 80 °C.

2.5 Compressive test

For a compressive test, the samples were cut into the cylindrical with a diameter of 3 mm and a length of 6 mm according to the ASTM E9–09 ($L/D=2.0$). Uniaxial compression tests were conducted at room temperature with a cross-head velocity of 0.2 mm/min on an electronic universal testing machine (WDW–50, Jinan Shijin Group Co., Ltd., China) to obtain the compressive strength and elastic modulus of the porous NiTi alloys. The superelasticity of the porous NiTi alloys was tested

on an Instron 3365 testing machine with a constant rate of 0.5%/min under the pre-strains of 3%, 5%, 8% and 10%, respectively.

2.6 Damping capacity test

The internal friction value of the porous samples was measured by a dynamic mechanical analyzer (DMA, Q800) in single-cantilever mode at a strain amplitude of 1.1×10^{-4} (amplitude of 10 μm) and a frequency of 0.1 Hz, ranging from –50 to 120 °C with constant heating and cooling rates of 5 °C/min. The dimension of the sample is cut into 35 mm × 4 mm × 0.8 mm.

3 Results and discussion

3.1 Effect of sintering temperatures on microstructure and mechanical properties of porous NiTi alloys

The optical micrographs of the porous NiTi alloys prepared with 3 wt.% Mg at different sintering temperatures are shown in Fig. 2, and the pore size distribution, density and porosity are shown in Fig. 3. A large number of pores with varied sizes are randomly distributed over the surface of porous NiTi alloys. It can be seen from Fig. 3(a) that with increasing the sintering temperature, the number of small pores (<20 μm) gradually increases first, reaching the maximum value at 900 °C, and then decreases sharply. While the number of medium pores (20–100 μm) gradually decreases, and there is little difference in the number of large pores (>100 μm). At the same time, the densities of the porous NiTi alloys gradually increase and the porosities decrease with increasing the sintering temperatures, as seen in Fig. 3(b). When the sintering temperature is lower than 900 °C, lots of pores are derived from the interparticle pores due to the incomplete sintering [13,25], resulting in irregular pores and

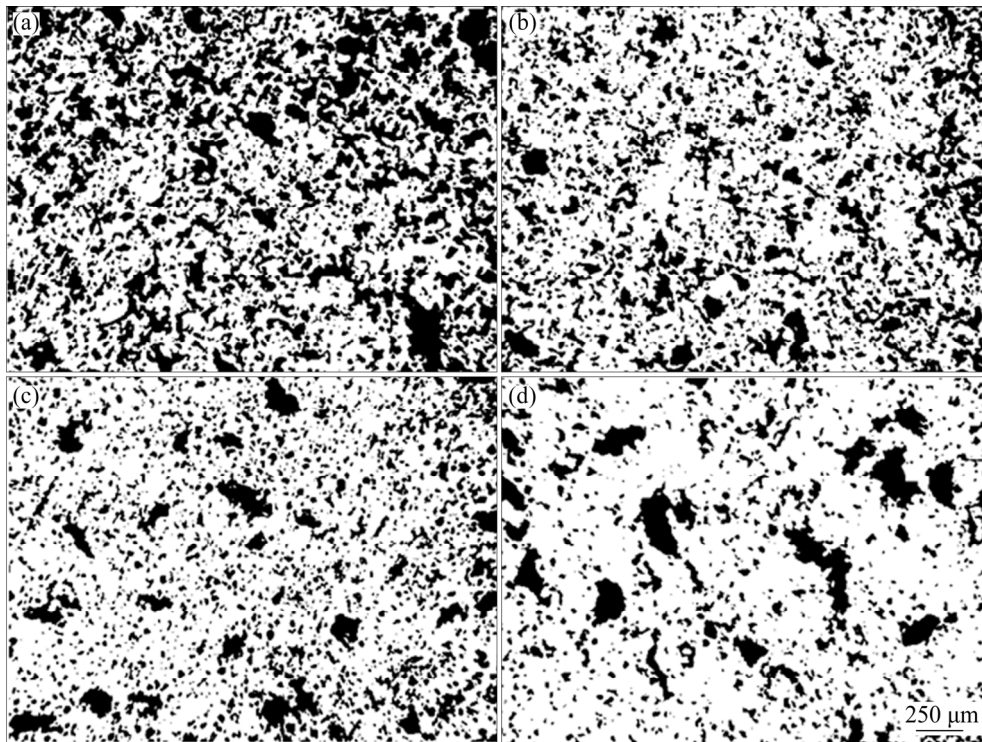


Fig. 2 Optical micrographs of porous NiTi alloys prepared with 3 wt.% Mg at different sintering temperatures: (a) 800 °C; (b) 850 °C; (c) 900 °C; (d) 950 °C

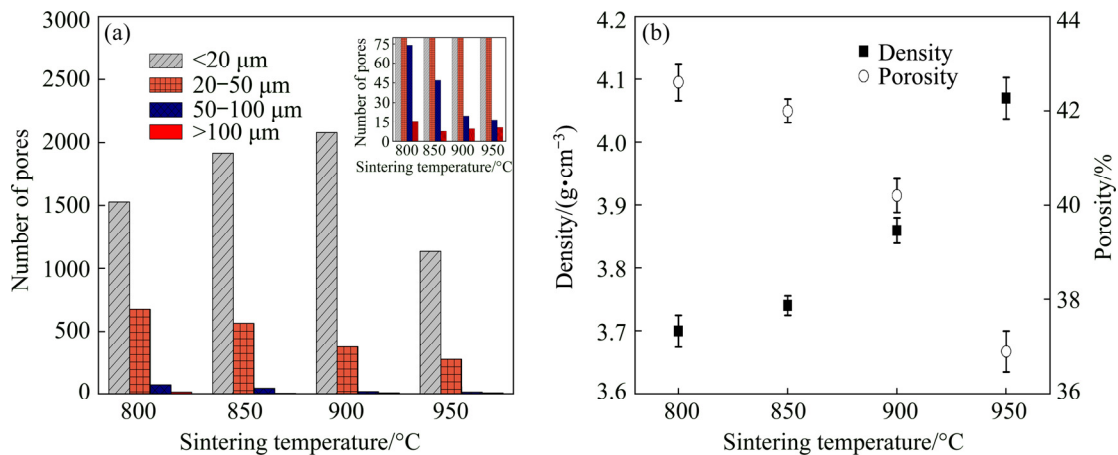


Fig. 3 Pore size distribution (a), density and porosity (b) of porous NiTi alloy prepared with 3 wt.% Mg at different sintering temperatures

good connectivity. As the sintering temperature is up to 950 °C, the partial melting occurs during the sintering process, leading to the sharp decrease of the small pores and the increase of the inhomogeneous large pores [26], as seen in Fig. 2(d). Therefore, the sintering temperature of 900 °C is appropriate to allow the porous NiTi alloy to be fully sintered without oversintering.

In the initial stage of sintering, the sintering necks are only formed at the points of the contact between the particles [27]. As the sintering

temperature increases, the atoms of the particles are thermally activated and the mass diffusion occurs, which promotes the growth of sintered necks to reduce the interparticle pores (medium pores), resulting in the porosities of the porous alloys decrease. However, excessive-high sintering temperature may lead to the partial melting of the compact, and the small pores are substantially eliminated (Fig. 3(a)). As a consequence, the shrinkage and densification of the sintered samples are further enhanced, leading to a decrease of the

porosities and the increase of the densities.

Figure 4 shows the XRD patterns of the porous NiTi–3Mg alloys prepared by the microwave sintering with 3 wt.% Mg at the different sintering temperatures. The porous NiTi–3Mg alloys are mainly composed of *B2* NiTi phase with a few *B19'* NiTi phase when the sintering temperature is lower than 950 °C, while two weak diffraction peaks assigned to the undesired secondary Ni_3Ti phase at $2\theta=46.4^\circ$ and $2\theta=43.4^\circ$ are detected when the sintering temperature is up to 950 °C, indicating that the porous NiTi–3Mg alloy prepared at 950 °C is also composed of a few Ni_3Ti phases except *B2* and *B19'* NiTi phases.

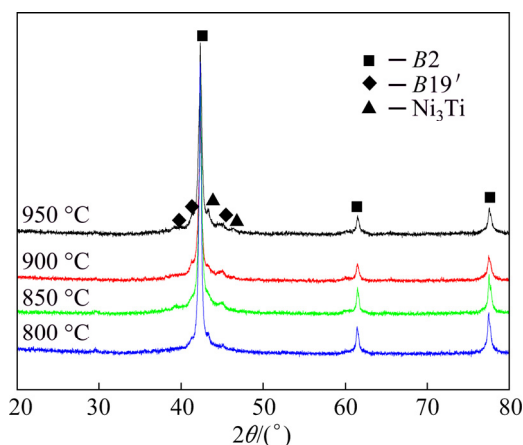


Fig. 4 XRD patterns of porous NiTi alloy prepared with 3 wt.% Mg at different sintering temperatures

According to Ti–Ni binary phase diagram [15], all of the NiTi, Ni_3Ti and Ti_2Ni are the equilibrium intermetallic phases in the near-equiatomic NiTi alloys, in which the Ni_3Ti is the most stable and the NiTi is the least stable based on the Gibbs free energy calculation [15]. Therefore, it is very difficult to obtain a single NiTi phase by the traditional solid-state sintering method. XU et al [12] and TANG et al [13] reported that the porous NiTi alloys prepared by microwave sintering also contained the undesired secondary phases. However, BISWAS [28] obtained the single-phase porous NiTi alloy using the high-temperature synthesis (SHS) method accompanied by the post-reaction heat treatment (a very low heating rate of 1 °C/min up to 1150 °C for 1 h). BERTHEVILLE [29] prepared the single-phase porous NiTi alloy using a vapor phase Ca reduction process under conventional sintering at 1000 °C for 2 h. Recently, ZAKI and ABDULLAH [30] also have obtained the

single NiTi phase in a solid-state reducing environment of CaH_2 at 930 °C for 3 h. Both the additions of Ca and CaH_2 indicate that the decrease of oxygen partial pressure inhibits the formation of secondary phases and the reducing atmosphere is very favorable for the formation of the single NiTi. In this study, the addition of Mg powders plays a key role in the formation of the single-phase porous NiTi alloy. Firstly, the melting point of Mg is only 650 °C, while the sintering temperature of the porous NiTi alloy is up to 900 °C. During the sintering process, Mg changes into the liquid phase first and then volatilizes slowly. The addition of Mg plays the role of sintering assistant, which is extremely beneficial to promoting the rearrangement and mass transfer of Ti and Ni particles, thus accelerating the elemental diffusion and alloying process, and the formation of the single NiTi phase finally. Secondly, the strong oxygen affinity of Mg provides a reduction environment for the sintering of Ni–Ti compact, similar to the above-mentioned CaH_2 , which can be beneficial to obtaining the single NiTi phase. Moreover, the microwave field can greatly accelerate the atomic diffusion and efficiently impede the formation of secondary phases [31,32].

The typical compressive stress–strain curves of the porous NiTi alloy prepared with 3 wt.% Mg at different sintering temperatures are shown in Fig. 5, and the compressive strength and elastic modulus of the porous NiTi–3Mg alloys extracted from the stress–strain curves are shown in Fig. 6. The compressive stress–strain curves of the porous NiTi–3Mg alloys are quite different from the other porous alloys in Refs. [12,14,33], in which no obvious linear elastic deformation region can be detected as well as the stress plateau. Moreover, the porous NiTi–3Mg alloys exhibit an excellent compression plasticity, confirmed by the high maximum strains, higher than 40%, even up to 60% for the 900 °C sintered samples. It can be seen from the stress–strain curves that with increasing the sintering temperatures, the ultimate stress of the porous NiTi–3Mg alloys increases first, reaching a maximum value at 900 °C, and then decreases, indicating that the compressive strength also increases first, reaching a maximum value of 1881 MPa at 900 °C, and then decreases, as seen in Fig. 6. When the sintering temperature is lower than 900 °C, there are many interparticle pores in the

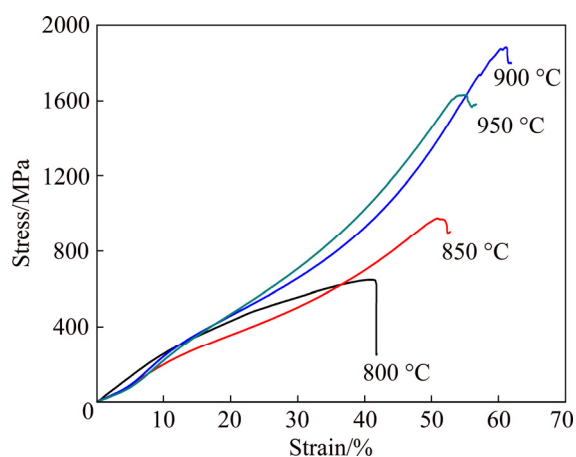


Fig. 5 Typical compressive stress–strain curves of porous NiTi alloy prepared with 3 wt.% Mg at different sintering temperatures

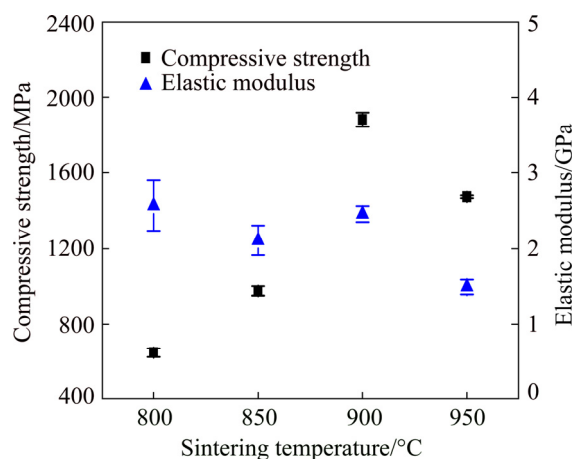


Fig. 6 Compressive strength and elastic modulus of porous NiTi alloy prepared with 3 wt.% Mg at different sintering temperatures

porous NiTi–3Mg alloys due to incomplete sintering, which are not conducive to the support of porous NiTi–3Mg alloy framework, leading to a relatively low compressive strength. While as the sintering temperature is up to 950 °C, the compressive strength decreases due to the stress concentration caused by the partial large pores and the formation of the secondary Ni₃Ti phase [34]. In addition, the sintering temperatures have little effect on the elastic modulus of the porous NiTi–3Mg alloys, which ranges from 1.5 to 2.5 GPa, keeping a low level. As a consequence, considering the factors of pore structure, phase composition and compressive strength, the sintering temperature of porous NiTi alloy prepared by microwave sintering with Mg space holder is optimized at 900 °C.

3.2 Effect of Mg content on microstructure and mechanical properties of porous NiTi alloys

Figure 7 shows the optical micrographs of the porous NiTi alloys sintered at 900 °C with different Mg contents, and the pore size distribution, density and porosity are shown in Fig. 8. It can be seen from Fig. 7 and Fig. 8(a) that there are only a large number of smaller pores (<50 μm) distributed over the surface of the porous NiTi–0Mg sample, and the number of larger pores (>50 μm) gradually increases with increasing the Mg content. Among the pores, the large pores (>50 μm) are mainly attributed to the residual pores of Mg volatilization [14]. The small pores (<20 μm) are commonly derived from the sintering necks and the Kirkendall pores [12,14,15]. Compared with the porous NiTi–xMg alloy, the number of the small pores distributed over the surface of the porous NiTi–10N drastically decreases and the average size of the large pores (>100 μm) is up to 165 μm, even larger than the size of NH₄HCO₃ particles. The large pores on porous NiTi–10N sample are derived from the decomposition of NH₄HCO₃ particles, and pore sizes are always dependent on the geometrical heredity of NH₄HCO₃ particles [12,23,35]. Some of pores connect (see Fig. 7(f)), resulting in the average size of pores is higher than that of the NH₄HCO₃ particles [12]. The average size (approximately 120 μm) of the large pores (>100 μm) on the porous NiTi–xMg samples smaller than the Mg particle size may be attributed to the shrinkage of the samples during the sintering process.

The porosities of the porous NiTi–xMg alloys linearly increase with increasing the Mg content, while the density accordingly decreases, as seen in Fig. 8(b). The porosity of the porous NiTi–0Mg alloy is only 21.5%, while the porosity fleetly increases to 37.8% for the porous NiTi–1Mg alloy, and linearly increases to 47.1% for the porous NiTi–7Mg alloy. However, with further increasing the Mg content, the NiTi compacts are difficult to alloy. On the other hand, the density decreases from 5.06 g/cm³ for NiTi–0Mg alloy to 3.41 g/cm³ for the porous NiTi–7Mg alloy. This result is greatly consistent with the optical micrographs of the porous NiTi alloys. The higher the Mg contents are, the more residual large pores obtain, which inevitably leads to the increase of porosities and the decrease of densities. Moreover,

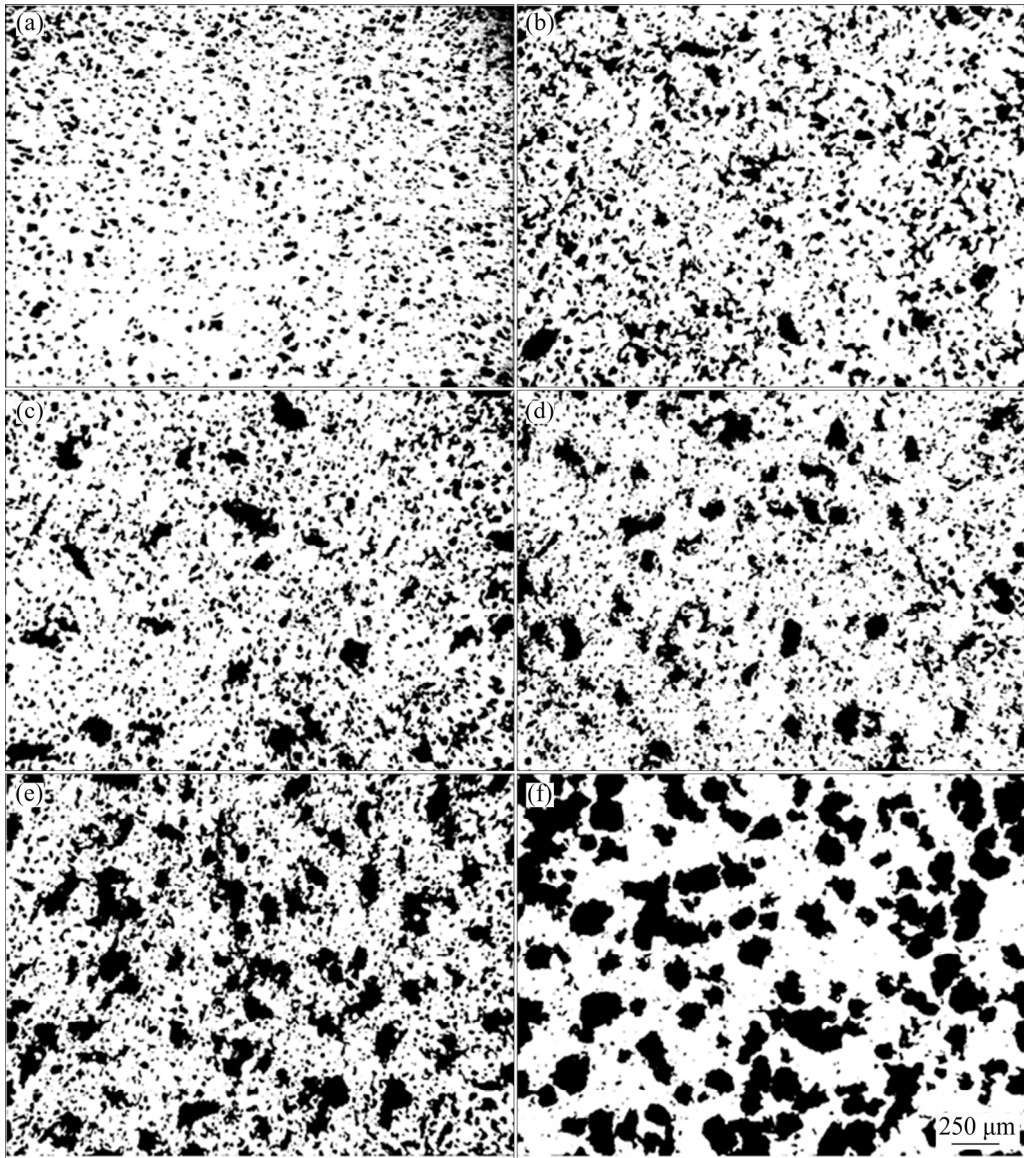


Fig. 7 Optical micrographs of porous NiTi alloys sintered at 900 °C with different Mg contents: (a) 0 Mg; (b) 1 Mg; (c) 3 Mg; (d) 5 Mg; (e) 7 Mg; (f) 10N

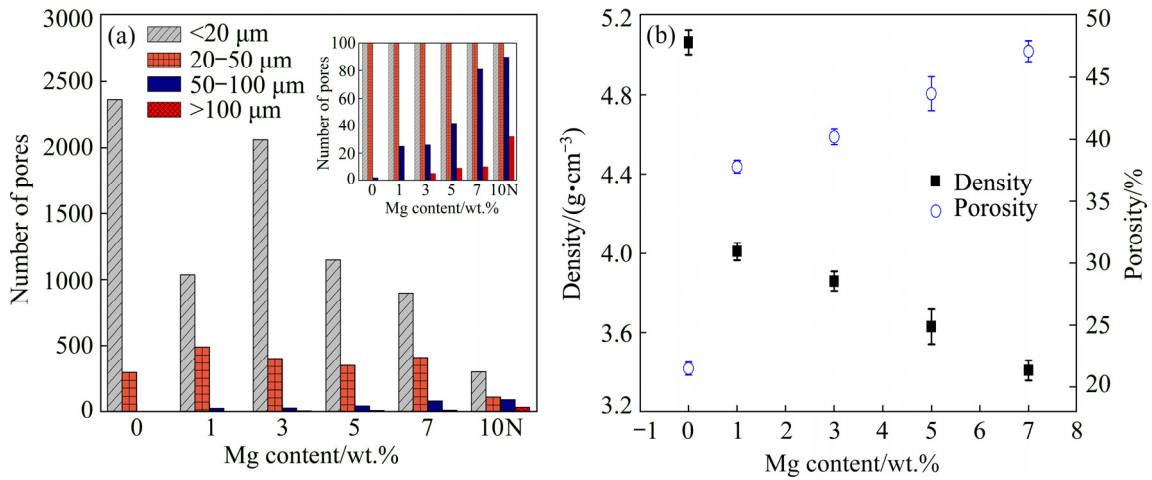


Fig. 8 Pore size distribution (a), density and porosity (b) of porous NiTi alloy sintered at 900 °C with different Mg contents

the porosity of the porous NiTi–10N alloy is 42.9%, similar to the porosity of 43.7% for the porous NiTi–5Mg alloy. The number of the larger pores (>50 μm) on the porous NiTi–10N alloy is much more than that on the porous NiTi–5Mg alloy, while the smaller pores (<50 μm) of the former is much less than the latter, indicating that the smaller pores play an important role in increasing the porosities of the porous NiTi alloy.

Figure 9 shows the effect of Mg content on the XRD patterns of the porous NiTi– x Mg alloys, with the NiTi–0Mg and NiTi–10N as controls. All of the porous NiTi– x Mg alloys are mainly composed of *B2* NiTi phase with a few *B19'* NiTi phase and the Mg content has little effect on the diffraction peaks. On the contrary, both the NiTi–0Mg and NiTi–10N alloys consist of the undesired secondary Ni_3Ti and Ti_2Ni phases except *B2* and *B19'* NiTi phases, which is consistent with most of the references [9,11–13,23]. Our previous study [12] found that the increase of space holder agent (NH_4HCO_3) contents would promote the formation of the secondary phases. Fortunately, increasing the magnesium content does not affect the phase composition of the porous NiTi alloys, although it increases the porosity during the microwave sintering process. This result further confirms that the addition of Mg powders plays a key role in the formation of the single-phase porous NiTi alloy.

The typical compressive stress–strain curves of the NiTi– x Mg and NiTi–10N alloys prepared at

900 °C are shown in Fig. 10, and the compressive strength and elastic modulus extracted from the stress–strain curves are shown in Table 1. All of the

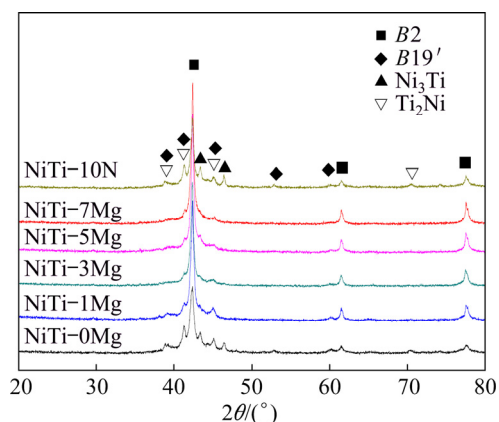


Fig. 9 XRD patterns of porous NiTi– x Mg and NiTi–10N alloys prepared at 900 °C

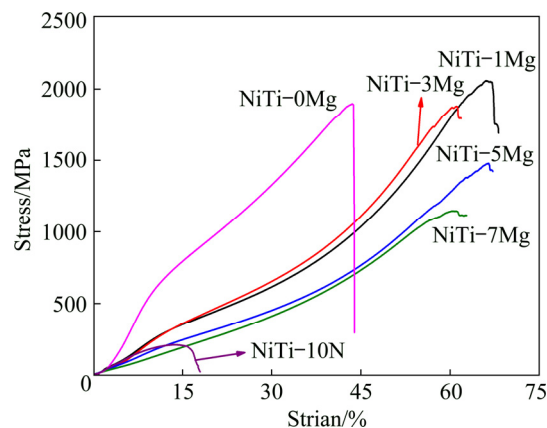


Fig. 10 Typical compressive stress–strain curves of porous NiTi– x Mg and NiTi–10N alloys prepared at 900 °C

Table 1 Comparison of phase composition and mechanical properties of porous NiTi alloy prepared under different methods in this study and references

Preparation method	Space holder agent	Porosity/%	Phase composition	σ /MPa	E /GPa	Ref.
MWS	–	21.5	NiTi, Ni_3Ti , Ti_2Ni	1898±127	6.8±0.08	This work
MWS	Mg	37.8	NiTi (<i>B2</i> , <i>B19'</i>)	2058±113	2.8±0.03	This work
MWS	Mg	40.2	NiTi (<i>B2</i> , <i>B19'</i>)	1881±38	2.5±0.1	This work
MWS	Mg	43.7	NiTi (<i>B2</i> , <i>B19'</i>)	1481±60	1.7±0.2	This work
MWS	Mg	47.1	NiTi (<i>B2</i> , <i>B19'</i>)	1146±43	1.4±0.01	This work
MWS	NH_4HCO_3	42.9	NiTi, Ni_3Ti , Ti_2Ni	212±13	3.6±0.1	This work
CS	Mg	39	NiTi, MgO	394±18	12.5±1.2	[14]
CS	–	24.6	NiTi, Ni_3Ti , Ti_2Ni , Ni	680	11	[36]
SHS	–	52.8	NiTi, Ni_4Ti_3 , Ti_2Ni	500	5.82	[37]
SHS	–	31.8	NiTi, Ni_4Ti_3 , Ti_2Ni	344±16	0.8–1.3	[38]
SPS	–	18	NiTi, Ni_3Ti , Ti_2Ni	1183	18.1	[11]
SPS	NH_4HCO_3	39	NiTi, Ni_3Ti , Ti_2Ni	260	12.5	[11]

E is elastic modulus; σ is compressive strength

maximum compressive strains of the porous NiTi- x Mg alloys are higher than 60% and the maximum strain of the NiTi-0Mg also reaches approximately 45%, while that of the NiTi-10N sample is only approximately 16%. The maximum stress of the NiTi- x Mg alloys gradually decreases with increasing the Mg content, indicating that the compressive strength of the NiTi- x Mg alloys also decreases with increasing the Mg content, as seen in Table 1. The compressive strength of the porous NiTi-1Mg sample ((2058±113) MPa) is higher than that of the porous NiTi-0Mg sample ((1898±127) MPa), although the porosity of the former (37.8%) is much higher than that of the latter (21.5%). For comparison, under the same porosity level (~43%), the compressive strength of porous NiTi-5Mg sample ((1481±60) MPa) is much higher than that of porous NiTi-10N sample ((212±13) MPa). At the same time, the compressive strengths of the porous NiTi- x Mg samples are much higher than those of other porous NiTi samples involved in the references [11,14,36–38], as shown in Table 1. Especially, the compressive strength of the porous NiTi- x Mg samples is higher than that of the dense Ti-6Al-4V ELI alloy (~1200 MPa) [33]. In addition, the elastic moduli of the porous NiTi- x Mg sample are ranged from 1.4 to 2.8 GPa, much lower than those of other porous NiTi samples, indicating that the porous NiTi- x Mg samples possess ultrahigh strength to modulus ratio and are very suitable for the orthopedic applications [39,40].

The high compressive strength of the porous NiTi- x Mg alloy with the porosities ranging from 37.8% to 40.2% is mainly attributed to the

following factors: (1) the single NiTi phase without Ti₂Ni and Ni₃Ti secondary phases can greatly improve the strength of porous NiTi alloy [34]; (2) the Mg powders as space holder material also play a sintering assistant role to remarkably reduce the sintering temperature of the porous NiTi alloy and realize the sufficient sintering; (3) the porous NiTi alloy is prepared by microwave sintering at a low sintering temperature for a short holding time (900 °C for 15 min), which can effectively inhibit the grain growth and realize the fine-grain strengthening [31,32].

3.3 Phase transformation behavior of porous NiTi alloys

Figure 11 shows the DSC curves of the porous NiTi-0Mg, NiTi-5Mg and NiTi-10N alloys, and the phase transformation peak values extracted from the DSC curves are listed in Table 2. Two exothermic peaks can be observed from the DSC curves of the NiTi-0Mg and NiTi-10N samples during the cooling process, indicating the two-step phase transformation of *B2* phase to *R* phase and *R* phase to *B19'* phase might occur. While only one exothermic peak at 6.1 °C can be detected from the DSC curve of the NiTi-5Mg sample, in which one-step phase transformation of *B2* phase to *B19'* phase should occur. Moreover, the M_p value of the NiTi-5Mg sample is a little lower than those of the NiTi-0Mg and NiTi-10N samples, which illustrates that the Mg space holder slightly reduces the martensitic transformation temperature of the porous NiTi alloys. During the heating process, two-step phase transformation of *B19'* phase to *R* phase and *R* phase to *B2* phase occurs at the

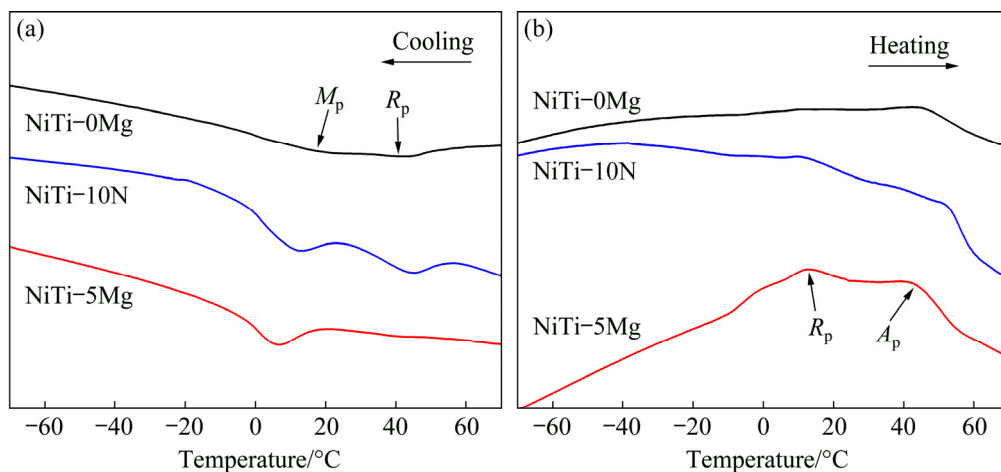


Fig. 11 DSC curves of porous NiTi-0Mg, NiTi-5Mg and NiTi-10N alloys

Table 2 Phase transformation peak values of porous NiTi alloys

Sample	Cooling process		Heating process	
	$R_p/^\circ\text{C}$	$M_p/^\circ\text{C}$	$R_p/^\circ\text{C}$	$A_p/^\circ\text{C}$
NiTi–0Mg	43.1	14.4	–	45.1
NiTi–5Mg	–	6.1	12.8	44.1
NiTi–10N	43.7	11.4	11.6	51.8

R_p , M_p and A_p represent the peak values of R phase transformation, martensitic transformation and austenitic transformation, respectively

NiTi–5Mg and NiTi–10N samples, while the one-step phase transformation of $B19'$ phase to $B2$ phase should occur at the NiTi–0Mg sample. At the same time, the A_p value of the NiTi–5Mg sample is a little lower than those of the NiTi–0Mg and NiTi–10N samples once again. Combined with the results of the cooling process and heating process, the Mg space holder changes the phase transformation behavior of porous NiTi alloys and slightly reduces the phase transformation temperatures.

3.4 Superelasticity of porous NiTi alloys

In order to investigate the superelasticity of the porous NiTi alloys under different sintering conditions, the loading–unloading curves of the porous NiTi–0Mg, NiTi–5Mg and NiTi–10N alloys under the pre-strains of 3%, 5%, 8% and 10% are shown in Fig. 12, and the results extracted from the curves are listed in the Table 3. With increasing the pre-strain (ε_{pre}), all of the maximum stresses (σ_{max}) of porous NiTi alloys gradually increase, and the σ_{max} value of the porous NiTi–0Mg sample is much higher than those of the porous NiTi–5Mg and NiTi–10N samples at the same pre-strain. These results are exactly consistent with Fig. 10. At the same time, all of the superelastic recovery strains (ε_{SE}) of the porous NiTi alloys gradually increase, while the superelastic recovery ratio ($\varepsilon_{\text{SE}}/\varepsilon_{\text{pre}}$) gradually decreases with increasing the pre-strain. Moreover, the $\varepsilon_{\text{SE}}/\varepsilon_{\text{pre}}$ of the porous NiTi–5Mg sample is higher than that of the porous NiTi–10N sample at the same pre-strain but lower than that of the NiTi–0Mg sample. After unloading the 10% pre-strain, all of the porous samples were heated to 100 °C. Due to the shape memory effect, the shape memory recovery strain (ε_{SM}) of the porous NiTi–0Mg sample reaches 1.95%, about 50% of the residual strain (3.90%). The ε_{SM} is up to 3.30% for

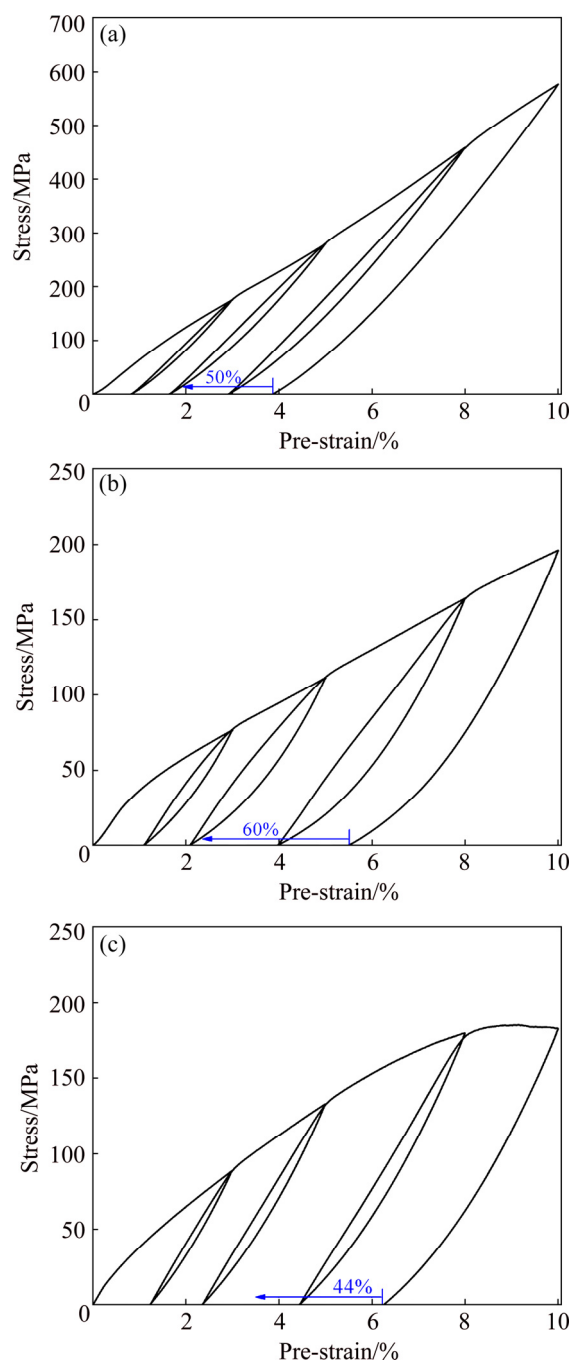


Fig. 12 Loading–unloading curves of porous NiTi–0Mg (a), NiTi–5Mg (b), and NiTi–10N (c) alloys under pre-strains of 3%, 5%, 8%, and 10%

the porous NiTi–5Mg sample, about 60% of the residual strain (5.50%), and it decreases to 2.76% for the porous NiTi–10N sample, about 44% of the residual strain (6.25%). Therefore, the shape memory recovery ratio of the porous NiTi–5Mg sample (60%) is higher than those of the porous NiTi–0Mg (50%) and NiTi–10N (44%) samples. According to the above-mentioned results, it can be seen that the porous NiTi alloys prepared with Mg

space holder have better superelasticity and shape memory effect than that of the porous NiTi sample prepared with NH_4HCO_3 space holder under the same porosity of $\sim 43\%$.

Table 3 Results of loading–unloading curves of porous NiTi–0Mg, NiTi–5Mg and NiTi–10N alloys

Sample	$\varepsilon_{\text{pre}}/\%$	$\sigma_{\text{max}}/\text{MPa}$	$\varepsilon_{\text{SE}}/\%$	$\varepsilon_{\text{SE}}/\varepsilon_{\text{pre}}$	$\varepsilon_{\text{SM}}/\%$
NiTi–0Mg	3	176.4	2.19	73%	–
	5	280.2	3.36	67%	–
	8	459.6	5.10	64%	–
	10	577.4	6.10	61%	1.95
NiTi–5Mg	3	76.7	1.90	63%	–
	5	111.6	2.92	58%	–
	8	164.2	4.03	50%	–
	10	196.2	4.50	45%	3.30
NiTi–10N	3	88.9	1.78	59%	–
	5	133.1	2.66	53%	–
	8	179.6	3.56	45%	–
	10	184.8	3.75	37%	2.76

3.5 Damping capacity of porous NiTi alloys

Figure 13 shows the internal friction (IF) versus temperature curves of the porous NiTi–0Mg, NiTi–5Mg and NiTi–10N alloys. Apparently, during the cooling process, the internal friction–temperature curves of NiTi–0Mg and NiTi–10N almost coincide, and they simultaneously reach the maximum value at -15.8°C , correspondingly the IF value of 0.093. The maximum value of internal friction of the porous NiTi–5Mg alloy appears at -21.3°C , correspondingly the IF value of 0.145. The maximum values of internal friction during the cooling process are mainly attributed to the martensitic phase transformation (see Fig. 11). Moreover, there is a small peak at 32°C in the internal friction–temperature curves of NiTi–0Mg and NiTi–10N due to the existence of *R* phase transformation. ZHANG and ZHANG [41] reported that the internal friction of dense NiTi alloy under the same experimental conditions was 0.100. Both the internal friction values of the porous NiTi–0Mg and NiTi–10N are a little lower than that of the dense NiTi alloy, while the NiTi–5Mg is 1.45 times higher than that of dense NiTi alloy, indicating that the porous NiTi alloy prepared with Mg space holder not only improves the mechanical properties

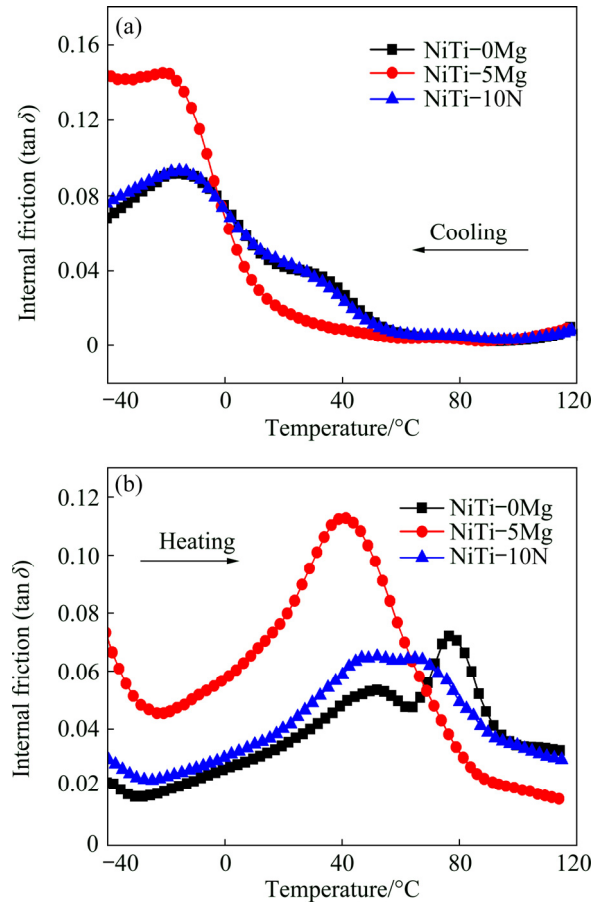


Fig. 13 Internal friction versus temperature curves of porous NiTi–0Mg, NiTi–5Mg and NiTi–10N alloys

and superelasticity, but also greatly enhances the damping capacity of the porous NiTi alloy. On the other hand, during the heating process, the maximum values of internal friction of the porous NiTi–5Mg, NiTi–0Mg and NiTi–10N alloys appear at 41.3 , 76.5 and 51.9°C , caused by the austenitic transformation, correspondingly the IF values of 0.113, 0.072 and 0.065, respectively, in which the IF value of the NiTi–5Mg is much higher than those of porous NiTi–0Mg and NiTi–10N alloys. Similarly, there are some small peaks in the internal friction–temperature curves due to the existence of *R* phase transformation during the heating process. GUO and KATO [42] prepared the submicroporous NiTi alloy by a top-down process with the IF value of 0.07, 40% higher than that fabricated by conventional powder sintering in Ref. [4], in which the authors considered that the fine pore structure increased the interface areas between the NiTi and pores and resulted in the higher IF value. Therefore, the high damping capacity of the porous NiTi–5Mg alloy in this work might be attributed to the single

NiTi phase and the unique pore structure increasing the interface areas between the NiTi and pores. However, the relationship between microstructure and damping capacity in the porous NiTi alloy should be studied systematically in the future.

4 Conclusions

(1) Porous NiTi shape memory alloys possessing the features of lightweight, high strength and high damping capacity were successfully prepared by microwave sintering using elemental Ti and Ni powders with Mg space holder.

(2) Except for a very small amount of Ni₃Ti phase in the samples sintered at 950 °C, all the porous NiTi alloys are composed of B2 NiTi phase with a few B19' NiTi phase, and the Ni₃Ti and Ti₂Ni secondary phases are eliminated.

(3) The Mg content has little effect on the phase composition of the porous NiTi alloys, but the Mg space holder changes the phase transformation behavior of the porous NiTi alloys. At the same time, the porosities of the porous NiTi alloys increase and the compressive strength decreases with increasing the Mg content.

(4) Compared with the porous NiTi alloy prepared with the NH₄HCO₃ space holder under the same porosity level, the porous NiTi alloy prepared with Mg space holder has much higher compressive strength, better superelasticity and shape memory effect and higher damping capacity.

Acknowledgments

The authors are grateful for the financial supports from the National Natural Science Foundation of China (51101085, 51764041, 51704167), the Aeronautical Science Foundation of China (2015ZF56027, 2016ZF56020), the Opening Project of National Engineering Research Center for Powder Metallurgy of Titanium & Rare Metals, China (2019004), the Key Laboratory of Lightweight and High Strength Structural Materials of Jiangxi Province, China (20171BCD40003), and the Jiangxi Provincial Natural Science Foundation, China (20202ACBL214011).

References

[1] ELAHINIA M, MOGHADDAM N S, ANDANI M T, AMERINATANZI A, BIMBER B A. Fabrication of NiTi

- through additive manufacturing: A review [J]. Progress in Materials Science, 2016, 83: 630–663.
- [2] XU J, TAO S, JIN X, LUO J, LIU Y. Effect of particle size on the microstructure and mechanical properties of the porous NiTi alloys prepared by microwave sintering [J]. Rare Metal Materials and Engineering, 2020, 49: 454–460.
- [3] ZHANG Yan-qiu, JIANG Shu-yong, ZHU Xiao-ming, ZHAO, Ya-nan, LIANG, Yu-long, SUN Dong. Influence of Fe addition on phase transformation behavior of NiTi shape memory alloy [J]. Transactions of Nonferrous Metals Society of China, 2017, 27: 1580–1587
- [4] LI D S, ZHANG X P, XIONG Z P, MAI Y W. Lightweight NiTi shape memory alloy based composites with high damping capacity and high strength [J]. Journal of Alloys & Compounds, 2010, 490: L15–L19.
- [5] BANSIDDHI A, SARGEANT T D, STUPP S I, DUNAND D C. Porous NiTi for bone implants: A review [J]. Acta Biomaterialia, 2008, 4(4): 773–782.
- [6] ARIFVIANTO B, ZHOU J. Fabrication of metallic biomedical scaffolds with the space holder method: A review [J]. Materials, 2014, 7(5): 3588–3622.
- [7] XIONG J Y, LI Y C, WANG X J, HODGSONPD, WEN C E. Titanium–nickel shape memory alloy foams for bone tissue engineering [J]. Journal of the Mechanical Behavior of Biomedical Materials, 2008, 1(3): 269–273.
- [8] SADRNEZHAAD S K, HOSSEINI S A. Fabrication of porous NiTi-shape memory alloy objects by partially hydrided titanium powder for biomedical applications [J]. Materials & Design, 2009, 30(10): 4483–4487.
- [9] SAADATI A, AGHAJANI H. Fabrication of porous NiTi biomedical alloy by SHS method [J]. Journal of Materials Science: Materials in Medicine, 2019, 30(8): 92.
- [10] WU S, CHUNG C Y, LIU X, CHU P K, HO J P Y, CHU C L, CHAN Y L, YEUNG K W K, LU W W, CHEUNG K M C, LUK K D K. Pore formation mechanism and characterization of porous NiTi shape memory alloys synthesized by capsule-free hot isostatic pressing [J]. Acta Materialia, 2007, 55(10): 3437–3451.
- [11] ZHANG L, ZHANG Y Q, JIANG Y H, ZHOU R. Superelastic behaviors of biomedical porous NiTi alloy with high porosity and large pore size prepared by spark plasma sintering [J]. Journal of Alloys and Compounds, 2015, 644: 513–522.
- [12] XU J L, BAO L Z, LIU A H, JIN X J, TONG Y X, LUO J M, ZHONG Z C. Microstructure, mechanical properties and superelasticity of biomedical porous NiTi alloy prepared by microwave sintering [J]. Materials Science and Engineering C, 2015, 46: 387–393.
- [13] TANG C Y, ZHANG L N, WONG C T, CHAN K C, YUE T M. Fabrication and characteristics of porous NiTi shape memory alloy synthesized by microwave sintering [J]. Materials Science and Engineering A, 2011, 258: 606–6011.
- [14] NAKAS G I, DERICIOGLU A F, BOR S. Monotonic and cyclic compressive behavior of superelastic TiNi foams processed by sintering using magnesium space holder

- technique [J]. *Materials Science and Engineering A*, 2013, 582: 140–146.
- [15] HEY J C, JARDINE A P. Shape memory TiNi synthesis from elemental powders [J]. *Materials Science and Engineering A*, 1994, 188(1–2): 291–300.
- [16] BAKHSHESHI-RAD H R, DAYAGHI E, ISMAIL A F, AZIZ M, AKHAVAN-FARID A, CHEN X. Synthesis and in-vitro characterization of biodegradable porous magnesium-based scaffolds containing silver for bone tissue engineering [J]. *Transactions of Nonferrous Metals Society of China*, 2019, 29: 984–996.
- [17] ZHENG Jing-pu, CHEN Liang-jian, CHEN Dai-yuan, SHAO Chun-sheng, YI Man-fei, ZHANG Bo. Effects of pore size and porosity of surface-modified porous titanium implants on bone tissue ingrowth [J]. *Transactions of Nonferrous Metals Society of China*, 2019, 29: 2534–2545.
- [18] BANSIDDHI A, DUNAND D C. Shape-memory NiTi foams produced by solid-state replication with NaF [J]. *Intermetallics*, 2007, 15(12): 1612–1622.
- [19] AYDOĞMUŞ T, BOR Ş. Superelasticity and compression behavior of porous TiNi alloys produced using Mg spacers [J]. *Journal of the Mechanical Behavior of Biomedical Materials*, 2012, 15: 59–69.
- [20] AYDOĞMUŞ T, BOR Ş. Processing of porous TiNi alloys using magnesium as space holder [J]. *Journal of Alloys and Compounds*, 2009, 478(1–2): 705–710.
- [21] JAKUBOWICZ J, ADAMEK G, DEWIDAR M. Titanium foam made with saccharose as a space holder [J]. *Journal of Porous Materials*, 2013, 20(5): 1137–1141.
- [22] CHEN G, CAO P, WEN G, EDMONDSN, LI Y. Using an agar-based binder to produce porous NiTi alloys by metal injection moulding [J]. *Intermetallics*, 2013, 37: 92–99.
- [23] XU J L, BAO L Z, LIU A H, JIN X J, LUO J M, ZHONG Z C, ZHENG Y F. Effect of pore sizes on the microstructure and properties of the biomedical porous NiTi alloys prepared by microwave sintering [J]. *Journal of Alloys and Compounds*, 2015, 645: 137–142.
- [24] KALANTARI S M, ARABI H, MIRDAMADI S, MIRSALEHI S A. Biocompatibility and compressive properties of Ti–6Al–4V scaffolds having Mg element [J]. *Journal of the Mechanical Behavior of Biomedical Materials*, 2015, 48: 183–191.
- [25] KOTAN G, BOR A S. Production and characterization of high porosity Ti–6Al–4V foam by space holder technique in powder metallurgy [J]. *Turkish Journal of Engineering & Environmental Sciences*, 2014, 31(3): 149–156.
- [26] DEWIDAR M, MOHAMED H F, LIM J K. A New approach for manufacturing a high porosity Ti–6Al–4V scaffolds for biomedical applications [J]. *Journal of Materials Science and Technology*, 2008, 24(6): 931–935.
- [27] WANG X, LI Y, XIONG J, HODGSONPD, WEN C. Porous TiNbZr alloy scaffolds for biomedical applications [J]. *Acta Biomaterialia*, 2009, 5(9): 3616–3624.
- [28] BISWAS A. Porous NiTi by thermal explosion mode of SHS: Processing, mechanism and generation of single phase microstructure [J]. *Acta Materialia*, 2005, 53(5): 1415–1425.
- [29] BERTHEVILLE B. Porous single-phase NiTi processed under Ca reducing vapor for use as a bone graft substitute [J]. *Biomaterials*, 2006, 27(8): 1246–1250.
- [30] ZAKI M H H, ABDULLAH J. The role of CaH₂ in preventing oxidation for the production of single-phase NiTi alloy in solid state [J]. *Journal of Alloys and Compounds*, 2016, 31: 188–197.
- [31] KHALED D E, NOVAS N, GAZQUEZ J A, AGUGLIARO F M. Microwave dielectric heating: Applications on metals processing [J]. *Renewable and Sustainable Energy Reviews*, 2018, 82: 2880–2892.
- [32] MISHRA R R, SHARMA A K. Microwave-material interaction phenomena: Heating mechanisms, challenges and opportunities in material processing [J]. *Composites Part A: Applied Science & Manufacturing*, 2016, 81: 78–97.
- [33] ESEN Z, BOR Ş. Characterization of Ti–6Al–4V alloy foams synthesized by space holder technique [J]. *Materials Science and Engineering A*, 2011, 528: 3200–3209.
- [34] OTSUKA K, REN X. Recent developments in the research of shape memory alloys [J]. *Intermetallics*, 1999, 7(5): 511–528.
- [35] LI D S, ZHANG Y P, MA X, ZHANG X P. Space-holder engineered porous NiTi shape memory alloys with improved pore characteristics and mechanical properties [J]. *Journal of Alloys and Compounds*, 2009, 474(1–2): L1–L5.
- [36] ZHU S L, YANG X J, FU D H, ZHANG L Y, LI C Y, CUI Z D. Stress–strain behavior of porous NiTi alloys prepared by powders sintering [J]. *Materials Science and Engineering A*, 2005, 408(1–2): 264–268.
- [37] CHU C L, CHUNG C Y, LIN P H, WANG S D. Fabrication and properties of porous NiTi shape memory alloys for heavy load-bearing medical applications [J]. *Journal of Materials Processing Technology*, 2005, 169(1): 103–107.
- [38] WISUTMETHANGOON S, DENMUD N, SIKONG L. Characteristics and compressive properties of porous NiTi alloy synthesized by SHS technique [J]. *Materials Science and Engineering A*, 2009, 515(1–2): 93–97.
- [39] LIU Y, LI S, HOU W, WANG S, HAO Y, YANG R, SERCOMBE T B, ZHANG L C. Electron beam melted beta-type Ti–24Nb–4Zr–8Sn porous structures with high strength-to-modulus ratio [J]. *Journal of Materials Science & Technology*, 2016, 32(6): 505–508.
- [40] ZHOU Y L, LUO D M. Microstructures and mechanical properties of Ti–Mo alloys cold-rolled and heat treated [J]. *Materials Characterization*, 2011, 62(10): 931–937.
- [41] ZHANG Y P, ZHANG X P. Internal friction behaviors of porous NiTi alloys with variable porosities [J]. *The Chinese Journal of Nonferrous Metals*, 2009, 19(10): 1872–1879.
- [42] GUO W, KATO H. Submicron-porous NiTi and NiTiNb shape memory alloys with high damping capacity fabricated by a new top-down process [J]. *Materials & Design*, 2015, 78: 74–79.

镁造孔多孔 NiTi 合金的微波烧结制备与表征

赖涛¹, 徐吉林¹, 肖奇飞¹, 佟运祥², 黄俊¹, 张剑平¹, 罗军明¹, 刘勇³

1. 南昌航空大学 材料科学与工程学院, 南昌 330063;

2. 哈尔滨工程大学 生物医学材料与工程研究中心, 哈尔滨 150001;

3. 南昌大学 江西省轻质高强结构材料重点实验室, 南昌 330031

摘要: 为了获得轻质、高强和高阻尼的多孔 NiTi 合金, 采用微波烧结协同镁造孔技术制备多孔 NiTi 合金。考察多孔 NiTi 合金的显微组织、力学性能、相变行为、超弹性和阻尼性能。结果表明: 当烧结温度低于或等于 900 °C 时, 多孔 NiTi 合金主要由 B2 NiTi 相和少量 B19' NiTi 相组成。随着烧结温度的升高, 多孔 NiTi 合金的孔隙率逐渐降低, 而压缩强度先增加后下降, 在 900 °C 时获得最大值。随着造孔剂 Mg 的含量从 1% 增加到 7% (质量分数), 多孔 NiTi 合金的孔隙率从 37.8% 增加到 47.1%, 而压缩强度从 2058 MPa 降低至 1146 MPa。与碳酸氢铵造孔多孔 NiTi 合金相比, 镁造孔多孔 NiTi 合金的相变行为发生变化, 而压缩强度、超弹性、形状记忆效应和阻尼性能均获得极大的提高。

关键词: 多孔 NiTi 合金; 微波烧结; Mg 造孔; 超弹性; 阻尼性能

(Edited by Xiang-qun LI)